IEEE Photonics Journal
An IEEE Photonics Society Publication

Transient UV and Visible Luminescent Dynamics of Si-Rich SiO_x Metal–Oxide–Semiconductor Light-Emitting Diodes

Volume 4, Number 5, October 2012

Gong-Ru Lin, Senior Member, IEEE
Chung-Hsiang Chang
Chih-Hsien Cheng, Student Member, IEEE
Chih-I Wu
Po-Sheng Wang

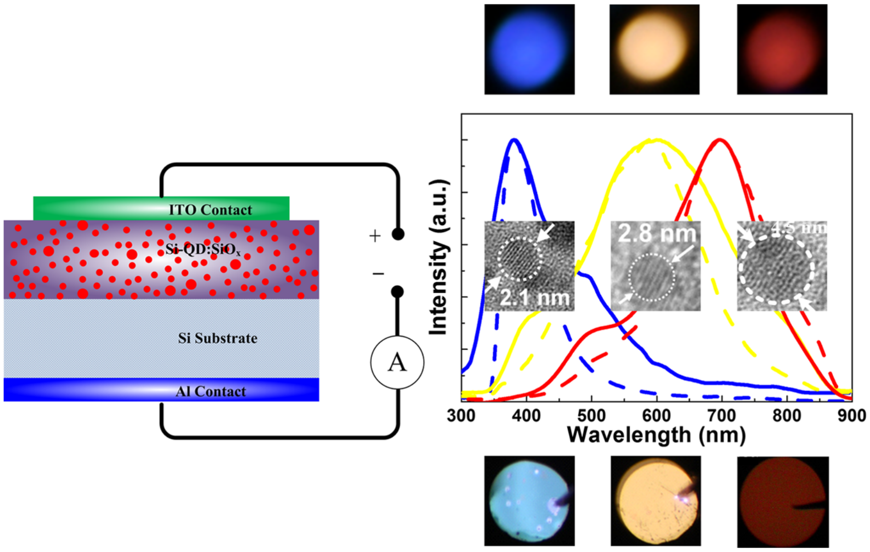

DOI: 10.1109/JPHOT.2012.2209633
1943-0655/$31.00

Transient UV and Visible Luminescent Dynamics of Si-Rich SiO_x Metal–Oxide–Semiconductor Light-Emitting Diodes

Gong-Ru Lin, *Senior Member, IEEE*, Chung-Hsiang Chang, Chih-Hsien Cheng, *Student Member, IEEE*, Chih-I Wu, and Po-Sheng Wang

Graduate Institute of Photonics and Optoelectronics, Department of Electrical Engineering,
National Taiwan University, Taipei 106, Taiwan

DOI: 10.1109/JPHOT.2012.2209633
1943-0655/$31.00 ©2012 IEEE

Manuscript received May 11, 2012; revised July 12, 2012; accepted July 16, 2012. Date of publication July 19, 2012; date of current version July 31, 2012. This work was partially supported by the National Science Council, Taiwan, and by the Excellent Research Projects of National Taiwan University, Taiwan, under Grants NSC 100-2221-E-002-156-MY3, NSC 101-2622-E-002-009-CC2, NSC 101-ET-E-002-004-ET, and 99R80301. Corresponding author: G.-R. Lin (e-mail: grlin@ntu.edu.tw).

Abstract: The transient ultraviolet (UV) and visible luminescent dynamics of the metal–oxide–semiconductor light-emitting diodes (MOSLEDs) made on Si-rich SiO_x with its O/Si composition ratio detuning from 0.75 to 1.62 are investigated. The size and luminescent wavelength of the buried Si quantum dots (Si-QDs) are controlled by adjusting the O/Si composition ratio of the Si-rich SiO_x. Time-resolved photoluminescence shows a lifetime decaying from 11.5 μs to 67 ns with the Si-QD size reducing from 4.5 to $>$ 1.7 nm. The shorter lifetime for smaller Si-QDs is due to the increased nonphonon-assisted carrier recombination rate in smaller Si-QDs. The Si-QD size shrinkage is obtained by enlarging the O/Si composition ratio via the increase in the N_2O/SiH_4 fluence ratio during synthesis, which makes the SiO_x matrix approaching a standard dioxide with a higher turn-on threshold field under Fowler–Nordheim tunneling. By increasing the O/Si composition ratio from 1.15 to 1. 54, the obtained EL pattern changes its color from red to blue, which is associated with the turn-on voltage increasing from 40 to 175 V. Decreasing the Si-QD size to 1.7 nm inevitably attenuates the EL power to 100 nW and reduces the P/I slope to 0.63 mW/A. The UV EL patterns of MOSLEDs made on the $SiO_{1.62}$ film are demonstrated with an EL power of 40 nW, and the decay of ITO transmittance to $<$ 30% at an EL wavelength of $<$ 375 nm also contributes to the power attenuation.

Index Terms: Silicon nanophotonics, quantum dots and single molecules, light-emitting diodes.

1. Introduction

Near-infrared (NIR) photoluminescence (PL) and electroluminescence (EL) of Si quantum dots (Si-QDs) have been extensively studied due to their potential applications in Si-based light-emitting devices (LEDs) for the optical interconnects between electronic integrated circuits [1]–[6]. Up to now, Si-QDs can only be generated in a SiO_x host matrix by employing a high-temperature annealing process. Indeed, the high-temperature annealing needed to form the Si-QDs in SiO_x (SiO_x:Si-QDs) films is somehow a puzzling problem with regard to the processing compatibility of the complementary metal–oxide–semiconductor (CMOS) technology. Nevertheless, there are new observations in recent works that the as-grown Si-QDs can be embedded in Si-rich SiN_x-based LEDs without annealing [7], [8]. Although different synthesizing and annealing conditions have been comprehensively studied for improving the light emission from a Si-rich SiO_x film, plasma-enhanced chemical vapor deposition (PECVD) is still the most intriguing method to produce dense Si-QDs in a robust and stable SiO_2 matrix. To date, the record for the operational stability of nanoporous Si-based LEDs of up to 2 h has been reported by Gelloz *et al.* [9]. In comparison, high-temperature annealed Si-rich SiO_x with size-tunable Si-QDs has also shown a comparable lifetime of operation, which is due to the relatively stable and saturated oxygen environment within the surrounding SiO_2 matrix [10].

In addition, versatile synthesizing and annealing recipes have also been proposed to obtain band gap tunable Si-QD and to improve the internal and external quantum efficiencies [11]–[14]. Previously, a Si nanostructure with a PL-related internal quantum efficiency (IQE) of 30%–50% has been measured by Atwater's group [11], [12]. Moreover, the maximum IQE of Si-QDs embedded in a SiO_2 host matrix is as high as $59 \pm 9\%$ [12]. A PL-related IQE of similar Si nanocrystals of several tens of percent has also been reported by the other groups [13], [14]. However, the EL-related external quantum efficiency (EQE) reported in previous works is much lower than the PL-related IQE. In the SiO_x:Si-QD-based metal–oxide–semiconductor light-emitting diodes (MOSLEDs), most of the electron–hole pairs contribute to the EL are injected into the Si-QDs through either impact excitation or the Fowler–Nordheim (F-N) tunneling process [15]. Although electron–hole recombination provides relatively similar EL and PL spectra, the EL-related EQE suffers from a limited tunneling probability of the carriers when passing through the SiO_x dielectric matrix [15]. As a result, only a few groups have reported an acceptable EL-related EQE ranging between 10^{-5} and 10^{-3} for Si-QD embedded MOSLEDs [4], [6], [16]–[18].

Nowadays, the fabricating technology of the MOSLEDs with red and infrared EL by tuning the Si-QD size is relatively mature [3], [19]–[21]. Marconi *et al.* employed a Si-QD/SiO_2 multilayer to form a MOSLED structure and observed EL at a wavelength of around 880 nm [20]. EL at shorter wavelengths of 700–780 nm was also demonstrated with Si-QD embedded SiO_x MOSLEDs [3]. However, only a few studies have emphasized obtaining the Si-QD-dependent PL emission at ultraviolet (UV) and blue regions [22], [23]. The difficulty arose by not only the precise control of Si-QD size and density but also the efficient pumping of small Si-QDs with a finite density of states [24]–[26]. Valenta *et al.* observed nearly coincident PL and EL spectra of an n^+-Si/SiO_x/p^+-Si diode [27]. Franzo *et al.* subsequently confirmed the luminescence caused by conduction-to-valence band recombination within a Si-QD [28]. Few current studies have addressed UV or blue EL emitted from any type of LED with buried Si-QDs.

This study preliminarily demonstrates blue and yellow EL emitted from MOSLEDs made on a Si-rich SiO_x film with buried Si-QDs. This approach is based on the precise control of quantum-confined Si-QD size by detuning the recipe of substrate temperature and N_2O/SiH_4 fluence ratio during PECVD synthesis. The variation of the O/Si composition ratio in SiO_x determines the quantity of excessive Si atoms in one SiO_2 unit cell so that the finite diffusion length of Si atoms in a Si-rich oxide matrix can be obtained. The excessive Si atom density and the diffusion length play important roles in confining the size Si-QDs after high-temperature annealing. Specifically, the variable diffusion lengths of Si atoms in Si-rich SiO_x films with changing O/Si composition ratios are correlated with the wavelength of EL produced by MOSLEDs.

2. Experimental Details

2.1. Preparation of Si-QD-Based Mosleds

The Si-rich SiO_x films were grown on a (100)-oriented p-type Si wafer using PECVD at a substrate temperature, chamber pressure, and RF plasma power of 250 °C–550 °C with 100 °C increments, 10 Pa, and 60 W, respectively. The SiH_4 and N_2O gaseous mixtures with changing fluence ratios were used as the reactant gas to deposit Si-rich SiO_x films with different O/Si composition ratios. The O/Si composition ratio is a nonlinear function of N_2O/SiH_4 fluence ratio. For

TABLE 1

O/Si composition ratio and Si-QD size versus the N_2O/SiH_4 fluence ratio and substrate temperature during PECVD growth

	N_2O/SiH_4 fluence ratio		
	(a): 6.8	(b): 4.5	(c): 2.3
Temperature	[O/Si] ratio / Si-QD size		
250°C	0.73/4.5	1.02/4.1	1.35/2.9
350°C	0.88/4.3	1.14/3.6	1.44/2.7
450°C	1.03/4.0	1.24/3.1	1.54/2.1
550°C	1.15/3.5	1.36/2.8	1.62/1.7

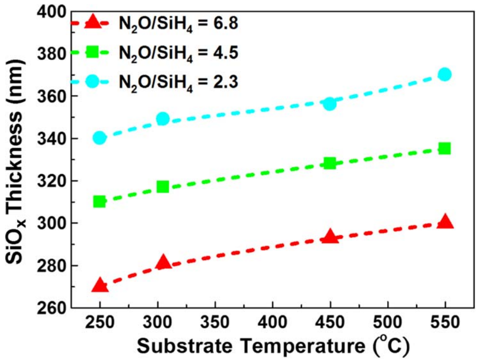

Fig. 1. (a) HRTEM image for the 1.7 ± 0.2 nm large Si-QDs embedded in a SiO_x sample with blue PL emission. (b) Size distribution of Si-QDs embedded in SiO_x films with blue PL emission. Inset: the magnified HRTEM image of the 1.7-nm large Si-QD.

samples grown with the (a) recipe with O/Si composition ratio of 0.73–1.15, the flowing rates of SiH_4 and N_2O gases were 11 sccm and 75 sccm, respectively. For Si-rich SiO_x samples grown with the (b) recipe with larger O/Si composition ratios of 1.02–1.37, the flowing rates of SiH_4 and N_2O gases were 11 sccm and 50 sccm, respectively. To obtain the Si-rich SiO_x samples with O/Si composition ratios of up to 1.42 or larger, the (c) recipe with N_2O gas fluence further decreased to 25 sccm at a constant SiH_4 fluence is used. This N_2O decreasing recipe facilitates Si-rich SiO_x growth for greater control on the size of Si-QDs. Table 1 lists the synthesizing recipes for all samples used in this work.

After deposition, the SiO_x films were annealed at 1100 °C in flowing N_2 (250 sccm) and H_2 (5 sccm) mixed gases for 90 min to induce Si-QD precipitation in the SiO_x matrix. The Si-QD size in Si-rich SiO_x is determined by using the high-resolution transmission electron microscopy (HRTEM, JEOL 2010). By taking the SiO_x:Si-QD film with blue PL as an example, the bright-field-view HRTEM image for the embedded Si-QDs is shown in Fig. 1(a). The size distribution of Si-QDs shown in Fig. 1(b) reveals that the Si-QD diameter is ranged between 1.2 and 2.2 nm, which exhibits a nearly Gaussian-like distribution function with its peak located at 1.7 nm and a full-width at half-maximum of 0.2 nm. Under illumination with a He-Cd laser at a wavelength and average intensity of 325 nm and 5 W/cm^2, respectively, the PL of Si-QDs buried in Si-rich SiO_x films ranging between 300 and 900 nm was resolved using a monochromator (CVI, DK240) connected to a photomultiplier (Hamamatsu R928) and a digital multimeter (HP 34401A). X-ray photoelectron spectroscopy (XPS) with a Mg K_α line illumination at 1253.6 eV was employed to analyze the O/Si composition ratio of Si-rich SiO_x films. A 200-nm-thick ITO film with a contact diameter of 0.8 mm was sputtered on the top of a Si-rich SiO_x surface, and a 500-nm-thick Al film was evaporated on the bottom of a p-Si substrate to form a MOSLED. The MOSLED was operated by a programmable electrometer (Keithley, model 6517) for EL characterization.

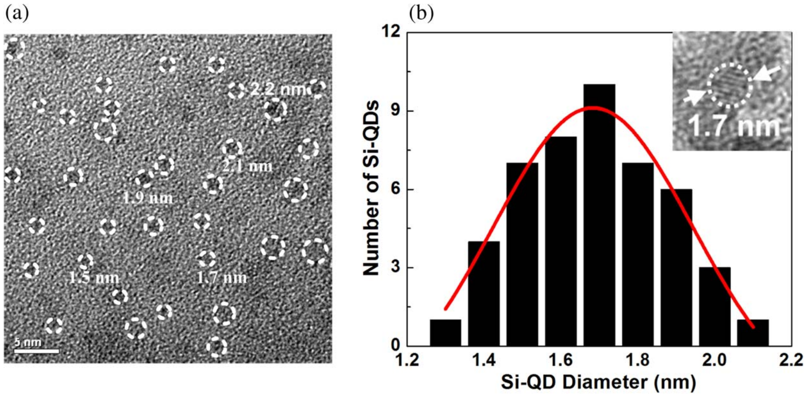

Fig. 2. Thickness of postannealed SiO_x samples grown with different recipes and substrate temperatures.

3. Results and Discussion

3.1. Thickness of Si-Rich SiO_x Films

The slight reduction in Si-rich SiO_x film thickness after annealing is mainly attributed to dehydrogenation, which becomes significant with lengthened annealing duration. With the same deposition and annealing durations, the $SiO_{0.75-1.14}$ film was thinner than the $SiO_{1.02-1.37}$ and $SiO_{1.42-1.62}$ films because of their increasing O/Si composition ratios. When increasing the deposition temperature under the same deposition time, the thickness of Si-rich SiO_x films grown with recipes (a), (b), and (c) slightly increased from 270 nm to 300 nm, 310 nm to 335 nm, and 340 nm to 370 nm, respectively, as shown in Fig. 2.

The Si-rich SiO_x thickness was also varied by changing the O/Si composition ratios because the sizes of Si and the O atom differentiate from each other significantly. Therefore, the thickness of Si-rich SiO_x films is a function of the volume ratio between self-assembled Si-QDs and standard SiO_2 so that the volumes of excessive Si atoms and standard SiO_2 in one mole of a Si-rich SiO_x film can be individually calculated to obtain the thickness of Si-rich SiO_x films. For example, the Si-rich SiO_x sample can be theoretically described as a function of self-assembled Si-QDs and standard SiO_2

$$\mathrm{SiO}_x \rightarrow \left(1-\frac{x}{2}\right)\mathrm{Si}+\frac{x}{2}\mathrm{SiO}_2. \tag{1}$$

By setting the O/Si composition ratio at 1.62 for Si-rich SiO_x films grown with recipe (c) at a substrate temperature of 550 °C, (1) shows that 0.19 moles $(1-x/2)$ of excessive Si atoms are buried in the 0.81 mole $(x/2)$ of standard SiO_2 molecules. Assuming that the unit cell volumes of SiO_2 and Si-QD are 13.996 and 0.16 nm^3, respectively, the volume of one mole Si-rich $SiO_{1.62}$ molecule is approximately 23.6 cm^3, as determined by

$$\mathrm{V}_{\mathrm{mole}}(\mathrm{SiO}_x) \approx \mathrm{V}_{\mathrm{mole}}(\mathrm{SiO}_2)+\mathrm{V}_{\mathrm{mole}}(\mathrm{Si}) \approx \frac{\frac{x}{2}\times N_0}{\mathrm{N}_{\mathrm{SiO}_2}}\times \mathrm{V}_{\mathrm{SiO}_2}+\frac{\left(1-\frac{x}{2}\right)\times N_0}{\mathrm{N}_{\mathrm{Si}}}\times \mathrm{V}_{\mathrm{Si}}. \tag{2}$$

Equation (2) shows both the estimated volume and the thickness of one mole Si-rich SiO_x film increase with the enlarging O/Si composition ratio (see Table 2). The standard variation of SiO_x thickness increases with the decreasing SiH_4/N_2O fluence ratio because of the enhanced decomposition process under the same RF plasma power. This causes the Si-rich SiO_x grown with recipe (c) to thicken more than the other samples grown with recipes (a) and (b) because of their higher O/Si composition ratios.

TABLE 2

Volume of one mole of Si-rich SiO_x molecule versus the N_2O/SiH_4 fluence ratio and substrate temperature during PECVD growth

	Volume of One mole SiO_x molecules (cm^3)		
Temperature	**(a): 6.8**	**(b): 4.5**	**(c): 2.3**
250°C	17.3	19.3	21.7
350°C	18.3	20.2	22.3
450°C	19.4	20.9	23.0
550°C	20.3	21.8	23.6

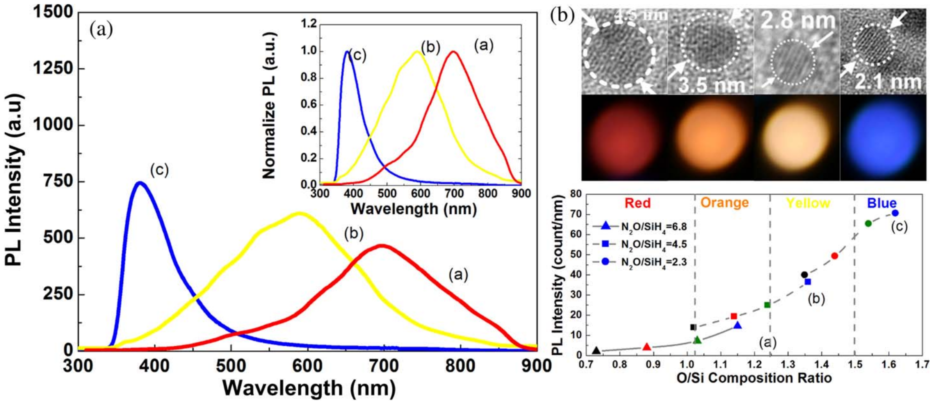

Fig. 3. (a) The actual and normalized (inset) PL of Si-rich SiO_x samples grown by changing the recipes (a) to (c) at a constant substrate temperature of 450 °C. (b) Top: PL emission patterns changing from red to blue corresponding to the change in average Si-QD size from 4.5 nm to 1.7 nm. Bottom: normalized PL intensity of a SiO_x sample grown with different recipes and substrate temperatures [250 °C (black), 350 °C (red), 450 °C (green), 550 °C (blue)] as a function of O/Si composition ratio. (All samples are annealed at 1100 °C for 90 min.)

3.2. PL Analysis of Si-QDs Embedded in Si-Rich SiO_x Films

Fig. 2 shows the PL spectra and related intensities of Si-rich SiO_x samples grown at different substrate temperatures (from 250 °C to 550 °C at 100 °C increment) and annealed at a constant duration of 90 min. At a constant substrate temperature, the PL peak wavelength exhibits a blue-shifted phenomenon with the growth recipe of N_2O/SiH_4 fluence ratio changing from (a) to (c), as Fig. 3(a) shows. As the O/Si composition increased from 1.42 to 1.62, the room-temperature PL peak wavelength of the Si-rich SiO_x sample blue-shifts to 350–410 nm and increases its intensity from 65 to 70 counts/nm. This is mainly attributed to the quantum confinement effect of Si-QDs as their size shrinks to 1.7–2.1 nm. The blue PL of the Si-rich SiO_x sample grown with recipe (c) is distorted by a sharp cut at the wavelength of approximately 350 nm caused by the high-pass filter in front of a monochromator, as Fig. 3(a) shows. Specifically, the PL peak wavelength centered at 760 nm for the Si-rich SiO_x sample grown with recipe (c) appears as an artificial signal because of the second-order harmonics of blue PL at 380 nm caused by a monochromator grating. Conversely, the PL peak wavelength further red-shifts to 580 nm with its linewidth greatly broadened to 200 nm as the O/Si composition ratio decreases to 1.37. The red PL of the Si-rich SiO_x sample grown with recipe (a) is slightly distorted because of the rapidly decayed spectral response of photomultiplier tubes (PMTs) at a wavelength exceeding 800 nm. When keeping the N_2O/SiH_4 fluence ratio constant, the Si-rich SiO_x samples grown at substrate temperature decreasing from 550 °C to 250 °C creates a red-shifted PL wavelength accompanied with a reduced PL peak intensity (normalized to Si-rich SiO_x film thickness), as Fig. 3(b) shows.

Fig. 3(b) shows the actual PL intensity normalized to the SiO_x thickness when comparing different samples because several samples are with slightly different thickness. Fig. 3(b) reveals that

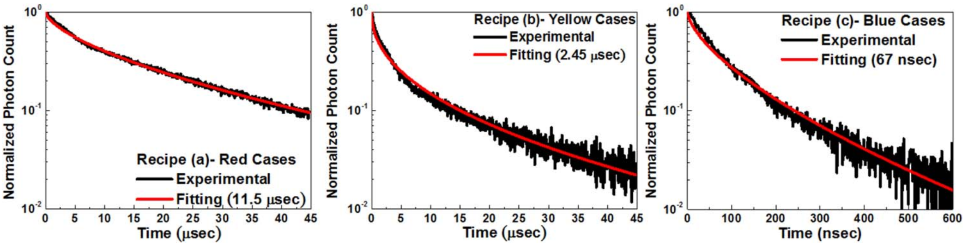

Fig. 4. TRPL traces for Si-QD embedded Si-rich SiO$_x$ films grown with recipes (a), (b), and (c).

a low-temperature growth usually results in both the decreased O/Si composition ratio and the red-shifted PL wavelength. Furthermore, the Si-rich SiO$_x$ sample grown at recipe (b) exhibits the O/Si composition ratio of 1.15–1.37 and the buried Si-QDs with size of 3.4–3.6 nm, which provides a white-yellow emission pattern with a weak PL peak intensity of 15–40 counts/nm. By further reducing the O/Si composition ratio to 0.73–1.15 with increasing N_2O gas fluence to 75 sccm, the 4.0–4.5-nm large Si-QDs contributed to an NIR PL with its peak wavelength and intensity red-shifted to 760–780 nm and decayed to 5–15 counts/nm, respectively. HRTEM images and PL patterns confirm that the PL color of the Si-rich SiO$_x$ film blue-shifts (red, orange, yellow, and blue) as the Si-QD size decreases (4.5 ± 0.3, 3.5 ± 0.2, 2.8 ± 0.3, and 2.1 ± 0.2 nm), which is relatively in good agreement with the theoretical prediction [29]. Although the SiO$_x$ samples have the identical O/Si composition ratio, the stronger PL of SiO$_x$ samples appears under higher N_2O/SiH_4 fluence ratio and lower substrate temperature. Because the SiO$_x$ samples become thicker when growing with lower N_2O/SiH_4 fluence ratio and lower substrate temperature, in which more Si-QDs can be precipitated to serve as the radiative luminescence center.

The invariant PL power from each Si-rich SiO$_x$ sample during a long-term test corroborates the stability of embedded Si-QDs. The luminescence contributed by most of the radiative defects can be ignored, including the weak oxygen bond (WOB, O–O) at 415 nm, the neutral oxygen vacancy (NOV, $O_3 \equiv \text{Si}-\text{Si} \equiv O_3$) at 455 nm, the E'_δ $(\text{Si} \uparrow \text{Si} \equiv \text{Si})$ at 520 m, and the nonbridged oxygen hole center (NOBHC, $O_3 \equiv \text{Si}-\text{O}\cdot$) at 630 nm [30]–[32]. In addition, the lack of nitrogen in a Si-rich SiO$_x$ matrix confirmed by XPS analysis also excludes other radiative recombination mechanisms, such as the Si–N bond transition at 428–477 nm, and the conduction-band to N_2^0-level (hole trap) or the N_4^+-level to valence-band (electron trap) transition at 413 nm [33], [34]. In general, these defects remain their PL wavelengths as constant and never vary with different SiO$_x$ sample recipes. In this case, the shift of PL wavelength (from PL analysis) in samples with different Si-QD size (from HRTEM analysis) is observed, and the proportionality between the PL wavelength and Si-QD is coincident with the theoretical simulation. The PL peak wavelengths of the samples are different from those of the radiative defects. These experimental results elucidate that even the radiative defects may have contributed to the PL, which is less compared with the contribution of the Si-QDs as the peak intensities of the defect-related PL component is insufficiently large to affect the whole PL spectrum. In addition, the blue PL exhibits a central peak wavelength at 380 nm in our case, which is apparently different from those wavelengths of the PL contributed by the radiative defects. From the average Si-QD size of 1.7 ± 0.2 nm, we can also correlate the PL peak wavelength and corresponding spectral linewidth with an empirical formula of $\lambda = 1.24/(1.12 + 5.83/d^{1.78})$ set for the Si-QDs buried in the SiO$_x$ matrix.

3.3. TRPL Analysis of Si-QDs Embedded in Si-Rich SiO$_x$ Films

The other evidence to distinguish the luminescence of Si-QDs from those of the radiative defects is the luminescent lifetime diagnosis of Si-QDs obtained from the time-resolved PL (TRPL) analysis. Fig. 4 shows the TRPL traces of three Si-rich SiO$_x$ samples pumped by a 10-ns gain-switched GaN laser diode pulse at 405 nm, which is detected by a PMT (Hamamatsu R928) with a switching response of 2–3 ns. In principle, the PL lifetime of the Si-QD embedded in the SiO$_x$ sample is strongly correlated with the radiative recombination rate of the electron–hole pairs inside the Si-QD.

Moreover, the Si-QD size distribution affects the dispersion factor (β) of the stretched exponential decay function in the fitting equation $\mathrm{I}(t) = I_0 \exp[-(t/\tau_{\mathrm{PL}})^{\beta}]$. τ_{PL} denotes PL lifetime, and β denotes dispersion factor correlated with Si-QD size distribution. With increasing Si-QD size distribution, the PL spectra become broadened and result in the enhanced lifetime dispersion phenomenon. Therefore, the broadened Si-QD size distribution contributes to the smaller dispersion factor (β). In this case, the single-stage stretched retention of the TRPL with a lower dispersion factor is employed to fit the oscilloscope trace of the time-resolved response of the full PL spectrum. The exponential decay constants of Si-QD-related luminescence for Si-rich SiO$_x$ samples grown with recipes (a), (b), and (c) are determined as 10.5 μs, 2.25 μs, and 67 ns, respectively. The PL decay time constant is decreased by more than two orders of magnitude when the Si-QD size shrinks from 4.5 nm to $<$ 1.7 nm. The dispersion factor of Si-QD-related luminescence for Si-rich SiO$_x$ samples grown with recipes (a), (b), and (c) are determined as 0.51, 0.62, and 0.73, respectively. By shrinking the Si-QD size of smaller than 8 nm, the enhanced momentum overlapping can be observed with further decreasing Si-QD size due to an increasing probability of nonphonon-assisted electron–hole recombination. A faster nonphonon-assisted electron–hole PL lifetime is mainly attributed to a larger momentum overlap between the electron and hole wave function in smaller Si-QDs, thus providing a higher recombination rate through the enhanced probability of direct transition [35]. We find that the lifetimes are consistent with electron–hole wave function overlap and momentum uncertainty.

The lifetime is usually contributed by nonradiative, radiative, and Auger recombinations. However, the TRPL can only determine the radiative lifetime and cannot be correlated with the nonradiative recombination process. During TRPL analysis, the radiative lifetimes of PL contributed by radiative defects and Si-QDs are different from each other. By decomposing the TRPL traces, we can distinguish the lifetime of radiative defects in the Si-rich SiO$_x$ film from that of the Si-QDs. The defect-related luminescence has been deconvoluted from the full-band TRPL traces shown in Fig. 4. Previously, the blue-band PL emission at 400–500 nm with lifetime of 5–37 ns due to oxygen-related defects at the Si-QD/SiO$_x$ interface was reported by Pi *et al.* and de Boer *et al.* [36], [37]. Moreover, the PL lifetime of E'_{δ} defect-related luminescence around 10 ns was reported by Nishikawa *et al.* [38]. In comparison, the PL lifetime of 67 ns obtained from the blue-color PL is much longer than those of defect-related luminescence. Therefore, the contribution of radiative defects has been taken into account, and the TRPL lifetimes reported in our work are not attributed to those defects [39]. The contribution of nonradiative defects is currently left as an unknown issue. This evidence further supports the direct radiative recombination in Si-QD core with a strong quantum confinement effect. For Si-rich SiO$_x$ samples with buried Si-QDs at different sizes, the strengthened PL intensity is observed and correlated with the reduced PL decay time constant. This result is straightforward by considering the PL intensity described as a function of the PL decay time and volume of Si-QDs [40]

$$I_{\mathrm{PL}} = \eta\sigma N_{\text{Si-QD}}\Phi(t)\frac{\tau_{\mathrm{pump}}}{\tau_{\mathrm{PL}}} \propto \mathrm{N}_{\text{Si-QD}}\Phi(t)\tau_{\mathrm{PL}}^{-1} \tag{3}$$

where I_{PL} is the Si-QD-related PL intensity, η is a relative coefficient, σ is an emission (absorption) cross section of radiative Si-QD, $\Phi(t)$ is the pumping flux density, τ_{pump} is the lifetime of pumping source, τ_{PL} is the radiative lifetime of Si-QD, and $\mathrm{N}_{\text{Si-QD}}$ is the volume density of recombination centers in Si-QDs.

3.4. XPS of Si-QDs Embedded in Si-Rich SiO$_x$ Films

The XPS analysis in Fig. 5 shows a linear variation of Si–O-related electron energy peak moving toward higher binding energy, indicating that the Si-rich SiO$_x$ matrix gradually changes to a pure SiO$_2$ structure after increasing the deposition temperature and N$_2$O fluence during growth [41]–[43]. The fitted XPS binding energy from 99.7 eV to 103.35 eV is attributed to the Si$_{(2p)}$ electrons from Si–Si bonds and O–Si–O bonds, respectively [44]. In this case, the XPS-binding peak of the Si-rich SiO$_x$ film with buried Si-QDs is caused by varying the O/Si composition ratio of the Si-rich SiO$_x$

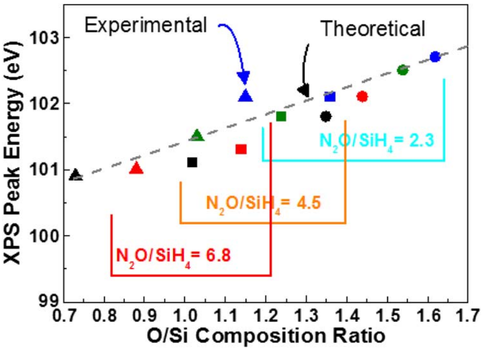

Fig. 5. XPS spectral peak energy of electrons from Si_{sp} core level versus the O/Si composition ratio of the SiO_x film grown by detuning the N_2O/SiH_4 fluence ratio and substrate temperature [250 °C (black), 350 °C (red), 450 °C (green), 550 °C (blue)].

matrix. Compared with $SiO_{1.42-1.62}$ and $SiO_{1.15-1.37}$ samples, a critical discrepancy between the N_2O fluence and total fluence occurs to vary the O/Si composition ratio of the Si-rich SiO_x film. The decomposition of a Si atom from SiH_4 is generally easier than that of an oxygen atom from N_2O because the desorption energies of N_2O and SiH_4 are 101.5 kcal/mol and 75.6 kcal/mol, respectively. When the PECVD chamber is filled with a lower molecule density of N_2O/SiH_4 mixture, the RF energy for each molecule given by the plasma in the PECVD chamber is high enough that the decomposition rates of O and Si atoms do not deviate significantly from each other. As the molecule density of the N_2O/SiH_4 mixture doubles by enlarging the reactant gas fluence, the reduced plasma energy on each molecule forces the decomposition of O and Si atoms to differentiate from each other. As a result, the anomalous growth of the Si-rich SiO_x film causes a higher excessive Si content. Thus, the O/Si composition ratio can be linearly detuned by changing the total N_2O/SiH_4 mixture fluence instead of the adjustment on the N_2O/SiH_4 fluence ratio. The increasing O/Si composition ratio inevitably results in a linear blue-shift of Si_{2p} X-ray photoelectron peak energy. Specifically, the deconvoluted peak intensity of Si–Si bonds within the Si_{2p} electron-related XPS signal also shows a decreasing trend as the O/Si composition ratio increases. This corroborates the reduced Si-QD density in a Si-rich SiO_x film grown with a lower N_2O/SiH_4 fluence ratio at a higher substrate temperature.

3.5. Voltage–Current Analysis of Si-QD-Based MOSLEDs

In addition, the voltage–current (*V*–*I*) analysis of Si-rich SiO_x MOSLEDs grown with different recipes and substrate temperatures is performed. The turn-on voltage and current defines the voltage required to turn on the tunneling the current and the EL emission, respectively. The *V*–*I* analysis shows that the threshold current for turning on MOSLEDs grown with recipe (b) is greatly reduced from 110 μA to 40 μA (see Fig. 6). The *V*–*I* plots illustrate the correlation of turn-on voltage and turn-on current of Si-rich SiO_x MOSLEDs with the O/Si composition ratio of the Si-QD-doped SiO_x film, as shown in the lower and upper part of Fig. 6. In Fig. 6, the short-dashed line with same color links the data of samples grown with a constant N_2O/SiH_4 fluence ratio, and the different patterns with same color indicate that the samples were grown at identical temperature. Consequently, the corresponding turn-on voltage of MOSLEDs grown with recipe (b) inevitably increases from 60 V to 140 V by enhancing the substrate temperature from 250 °C to 550 °C. In addition, the turn-on voltage and current of the MOSLEDs grown with recipes (a) and (c) have the same trends. In contrast, the Si-rich SiO_x-based MOSLEDs grown with recipe (a) exhibit the relatively low turn-on voltage and high injection current because of their extremely low O/Si composition ratios. However, the current passing across SiO_x-based MOSLEDs grown with recipe (c) decays significantly from 60 μA to 20 μA and is accompanied with increasing compliance voltages from 120 V to 225 V. The turn-on voltage and turn-on current of devices are dominated by the O/Si composition ratio in the Si-rich SiO_x film. The Si-rich SiO_x film gradually increases its

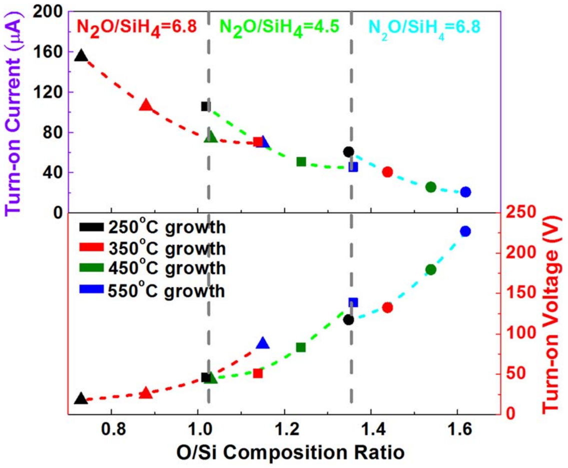

Fig. 6. Turn-on current (upper) and turn-on voltage (lower) of the SiO_x MOSLED versus the O/Si composition ratio of the Si-rich SiO_x film grown by detuning the $\mathrm{N_2O/SiH_4}$ fluence ratio as 6.8 (triangle patterns linked with red short-dashed line), 4.5 (square patterns linked with green short-dashed line), and 2.3 (circle patterns linked with blue short-dashed line) and by changing the substrate temperature as 250 °C (black patterns), 350 °C (red patterns), 450 °C (green patterns), and 550 °C (blue patterns).

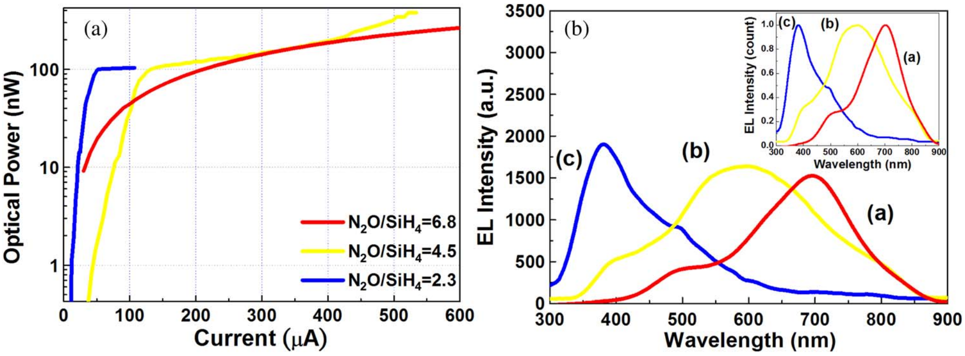

Fig. 7. (a) The P–I curves and (b) actual and normalized (inset) EL spectra of SiO_x-based MOSLEDs grown with recipes (a), (b), and (c) at substrate temperature 450 °C.

resistance with increasing the O/Si composition ratio because the Si-rich SiO_x film gradually becomes stoichiometric to approach a pure $\mathrm{SiO_2}$ matrix. A higher forward-biased condition is required to inject the carriers through the Si-rich SiO_x film with a higher O/Si composition ratio, and the tunneling-based carrier transport mechanism is dominated by exponential-like *V–I* behavior. In addition, the Si-rich SiO_x film with higher O/Si composition ratio easily contributes to smaller Si-QDs [45]. A smaller Si-QD decreases the effective dielectric constant and enhances the barrier height of F-N tunneling to degrade overall tunneling probability [46]. Therefore, the MOSLEDs decrease its turn-on current with increasing the O/Si composition ratio.

3.6. EL and Power–Current Analyses of Si-QD-Based MOSLEDs

The maximum output power of MOSLEDs made by SiO_x grown with recipes (a) and (b) are both up to 400 nW, and the corresponding P/I slopes are 0.63 mW/A and 0.91 mW/A, respectively [see Fig. 7(a)]. In addition, the $\mathrm{SiO}_{1.54}$-based MOSLED has an EL power of 100 nW at 40 μA with a P/I slope of 1.01 mW/A. The EL emission power of the Si-QD-doped SiO_x MOSLEDs grown with changing the recipe from (a) to (c) degrades because the carriers are hardly injected through the Si-rich SiO_x film with a higher O/Si composition ratio. Another reason is the limited ITO transmittance

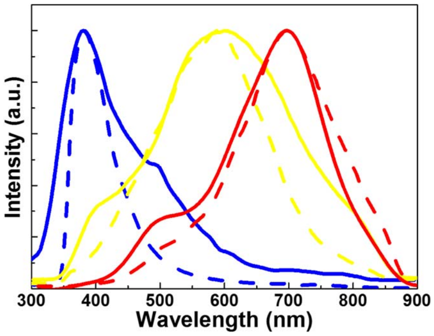

Fig. 8. PL (dashed line) and EL (solid line) spectra of Si-QD-based MOSLEDs with blue, yellow, and red color emissions grown with recipes (a), (b), and (c).

of 40%–50% in the blue region. The EQE is defined as the ratio of the output photon number and input electron number described as

$$\eta_{\text{ext}} = \int_{t_0}^{t_1} \frac{P(t)}{I(t)} \frac{e}{h\nu}\, dt = \frac{P_{opt}}{I_{\text{bias}}(1.24/\lambda)} \tag{4}$$

where P_{opt} defines the optical output power, λ defines the EL wavelength, and I_{bias} defines the bias current. The EQE of devices grown with recipe (a) increases from $5.4 \times 10^{-3}\%$ to $2.5 \times 10^{-2}\%$ with increasing substrate temperature from 250 °C to 550 °C. In addition, the EQE of devices grown with recipes (b) and (c) has same trends. The EQE of devices grown with recipes (b) and (c) enhances from $8.9 \times 10^{-3}\%$ to $3.6 \times 10^{-2}\%$ and from $3.2 \times 10^{-3}\%$ to $5.2 \times 10^{-2}\%$, respectively. The enhancement of EQE is mainly attributed to the stronger quantum confinement in smaller Si-QD. The stronger quantum confinement contributes to carriers confined in smaller Si-QDs to promote a higher probability of recombination. Therefore, the smaller Si-QD embedded SiO_x-based MOSLEDs have a higher EQE. Fig. 7(b) shows the EL spectra of MOSLEDs grown with the growth recipes changing from (a) to (c) at the biased electric field of 3.3 MV/cm, 6.7 MV/cm, and 8.8 MV/cm, respectively. It shows the primary EL peak wavelengths at 400–450 nm for blue MOSLEDs, at 600–650 nm for yellow MOSLEDs, and at 700–750 nm for red MOSLEDs. The blue-shifted phenomenon appears because the embedded Si-QD size decreases when increasing the O/Si composition ratio in the Si-rich SiO_x film. In addition, the EL spectra of MOSLEDs grown with recipes (a) and (b) are stronger and broader than those of the devices made with recipe (c) because the Si-rich SiO_x film with lower O/Si composition ratio has a broader Si-QD size distribution. Therefore, the devices with lower O/Si composition ratio easily have the secondary EL peak wavelengths due to the emission of small Si-QDs.

The EL and PL spectra of three different samples have been compared in Fig. 8. The central emission wavelength of EL and PL for all samples is not deviated from each other; however, there are some specific peaks observed in the EL spectrum. For the MOSLED with blue EL/PL, the EL peak wavelength centered at 380 nm is similar to PL peak wavelength. The sharpened PL at the short-wavelength side is due to the notch filter set for blocking the pumping laser spectrum. However, the EL linewidth of 126 nm is more broadened than the PL linewidth of 71 nm because another E'_δ defect (the precursor of Si-QDs) is also pumped under high biases [47]. In addition, the excessive carriers under a highly biased condition also excite the EL from larger Si-QDs with smaller volume density. Such a spectral broadening phenomenon has ever been discussed in previous work [47]. Similar trend is also observed in the other two samples. The yellow EL from the MOSLED driven at relatively high bias broadens its linewidth to 258 nm. A secondary EL peak decomposed with its peak located at around 400–405 nm results from the excitation of WOB defects in the incomplete SiO_x matrix with a small O/Si composition ratio. The highly biased

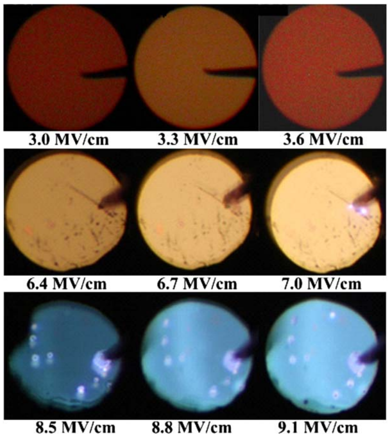

Fig. 9. EL emission patterns and biased field of SiO_x-based MOSLEDs grown at 450 °C with recipe (a) in upper row, (b) in middle row, and (c) in lower row.

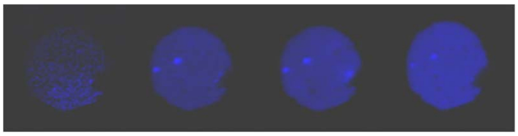

Fig. 10. UV EL patterns of $\mathrm{SiO}_{1.62}$-based MOSLEDs grown with recipe (c) at a substrate temperature of 550 °C (biased at 225–265 V from left to right at a 10-V increment).

operation also excites the larger Si-QDs in the yellow-EL MOSLED, whereas the weak E'_δ defect related radiation maybe covered by the broadband Si-QD-related EL spectrum. In the MOSLED with red-EL spectrum, the secondary EL peak at nearly 500–520 nm originated from the E'_δ defects is also observable in the PL spectrum [38].

The Si-QD-doped SiO_x MOSLEDs grown at a substrate temperature of 450 °C and the recipes (a), (b), and (c) show EL patterns in the upper, middle, and lower rows of Fig. 9, respectively. The EL pattern of the MOSLEDs changes its color from red to blue with increasing the $\mathrm{N_2O/SiH_4}$ fluence ratio because the Si-QD size decreases by increasing the O/Si composition ratio. To obtain sufficiently bright blue-EL emission patterns (immediately above the soft-breakdown regime), the forward bias was increased from 8.5 MV/cm to 9.1 MV/cm to elucidate that a higher turn-on voltage is required to tunnel the carriers through a Si-rich SiO_x film with a high O/Si composition ratio. In comparison, the EL patterns of devices grown with recipe (b) at a forward bias changing from 6.4 MV/cm to 7.0 MV/cm. In these MOSLEDs, the EL patterns become from dark yellow to bright yellow as the biased electrical field from 6.4 MV/cm to 6.7 MV/cm or larger. However, the yellow devices show an obvious soft-breakdown phenomenon at $>$ 7.0 MV/cm, which breaks down soon after a few minutes (1–3 min) when biasing above 7.5 MV/cm. A similar development of EL patterns from dark red to orange appears in the SiO_x-based MOSLEDs grown with recipe (a). Nevertheless, their bias electric field from 3.0 MV/cm to 3.6 MV/cm is substantially lower than those of the MOSLEDs made by other SiO_x samples with higher O/Si composition ratios. This phenomenon is corroborated by the decreased oxide resistance when growing the Si-rich SiO_x film with larger Si-QD size and lower O/Si composition ratio.

At last, Fig. 10 shows the UV EL patterns of $\mathrm{SiO}_{1.62}$-based MOSLEDs at a biasing voltage of up to 225–265 V. However, the top ITO contact degrades its transparency at UV-blue wavelengths to attenuate the EL power of UV MOSLEDs. The maximum EL power of a $\mathrm{SiO}_{1.62}$-based UV MOSLED is greatly attenuated to 35–40 nW when the ITO transmittance further decays to $<$ 30% when the EL wavelength blue-shifts to 375 nm or shorter [48]. The device lifetime is only 1–3 min for emitting EL at UV wavelength. The EL spectra of $SiO_{1.62}$-based MOSLEDs at different biases are unavailable because the overheating problem of UV MOSLEDs becomes severe at extremely high biases.

4. Conclusion

This study investigates the transient UV and visible luminescent dynamics of SiO_x-based MOSLEDs with different O/Si composition ratios grown by changing the N_2O/SiH_4 fluence ratio and substrate temperatures. The size and luminescent wavelength of Si-QDs can be controlled by adjusting the O/Si composition ratio precisely. By decreasing the N_2O fluence and the N_2O/SiH_4 fluence ratio from 75 to 25 sccm and from 6.8 to 2.3, respectively, TEM and XPS analyses reveal that the Si-QD size decreases from 4.5 to 1.7 nm as the O/Si composition ratio increases from 1.15 to 1.62. Substrate heating facilitates the growth of a Si-rich SiO_x film with a larger O/Si composition ratio, thus providing a small distribution range for Si-QD size and its PL wavelength. By shrinking the average size of Si-QDs from 4.5 to < 1.7 nm, the TRPL lifetime decay constant is significantly shortened from 11.5 μs to 67 ns. This is because of the larger overlap between electron and hole wave functions, which essentially leads to a faster nonphonon-assisted carrier recombination rate in smaller Si-QDs. Observations of both the continuous-wave and transient PL show that the direct radiative recombination process in Si-QD is the result of the strong quantum confinement effect rather than the oxygen-related defects. With the O/Si composition ratio between 0.8 and 1.15, the red EL pattern can be obtained from SiO_x-based MOSLEDs with relatively low turn-on voltage and high injecting current. The turn-on electric field of MOSLEDs inevitably increases when they are fabricated on a Si-rich SiO_x film with a larger O/Si composition ratio. The small Si-QDs with blue-shifted PL are obtained as the Si-rich SiO_x film gradually becomes stoichiometric to approach the standard SiO_2. Nevertheless, the density of Si-QDs decreases, and the F-N carrier tunneling threshold increases accordingly. To obtain a UV or blue EL from MOSLEDs made on a Si-rich SiO_x film with $x > 1.4$, the turn-on voltage and biased current are greatly increased to 225 V and decreased to 20 μA, respectively. To shorten the EL wavelength from 780 to $<$ 370 nm, the turn-on electric field incredibly increases from 3 to 9 MV/cm or higher. The maximum EL powers of 100 nW, 380 nW, and 400 nW for MOSLEDs with blue-, yellow-, and red-emission, respectively, are obtained with P/I slopes of 1.01 mW/A, 0.91 mW/A, and 0.63 mW/A, respectively. With a bias voltage of up to 225–265 V, the UV EL pattern can be observed from MOSLEDs made by $SiO_{1.62}$ with a buried Si-QD size of $<$ 1.7 nm. However, the EL power greatly attenuates to 40 nW or less because of the greatly attenuated transmittance of the top transparent ITO contact at UV wavelengths. The device lifetime is only 1–3 min for emitting EL at the UV wavelength. In the future, a multicolor MOSLED-based light source could be used in applications such as an alternative transmitter in an all-Si-based optical interconnect to improve the chip-to-chip transmission performance of Si-based microelectronics. With further enhancement on IQE and EQE, this type of light source could be used in other applications in Si-based microdisplay and microillumination chips.

References

[1] M. Wang, X. Huang, J. Xu, W. Li, Z. Liu, and K. Chen, "Observation of the size-dependent blueshifted electroluminescence from nanocrystalline Si fabricated by KrF excimer laser annealing of hydrogenated amorphous silicon/amorphous-SiN_x:H superlattices," *Appl. Phys. Lett.*, vol. 72, no. 6, pp. 722–724, Feb. 1998.

[2] O. Jambois, H. Rinnert, X. Devaux, and M. Vergnat, "Photoluminescence and electroluminescence of size-controlled silicon nanocrystallites embedded in SiO_2 thin films," *J. Appl. Phys.*, vol. 98, no. 4, pp. 046105-1–046105-3, Aug. 2005.

[3] G.-R. Lin and C. J. Lin, "CO_2 laser rapid-thermal-annealing SiO_x based metal–oxide–semiconductor light emitting diode," *Appl. Phys. Lett.*, vol. 91, no. 7, pp. 072103-1–072103-3, Aug. 2007.

[4] M. Perálvarez, C. García, M. López, B. Garrido, J. Barreto, C. Domínguez, and J. A. Rodríguez, "Field effect luminescence from Si nanocrystals obtained by plasma-enhanced chemical vapor deposition," *Appl. Phys. Lett.*, vol. 89, no. 5, pp. 051112-1–051112-3, Jul. 2006.

[5] S. Prezioso, A. Anopchenko, Z. Gaburro, L. Pavesi, G. Pucker, L. Vanzetti, and P. Bellutti, "Electrical conduction and electroluminescence in nanocrystalline silicon-based light emitting devices," *J. Appl. Phys.*, vol. 104, no. 6, pp. 063103-1–063103-8, Sep. 2008.

[6] K. S. Cho, N. M. Park, T. Y. Kim, K. H. Kim, G. Y. Sung, and J. H. Shin, "High efficiency visible electroluminescence from silicon nanocrystals embedded in silicon nitride using a transparent doping layer," *Appl. Phys. Lett.*, vol. 86, no. 7, pp. 071909-1–071909-3, Feb. 2005.

[7] L. Y. Chen, W. H. Chen, and F. C. N. Hong, "Visible electroluminescence from silicon nanocrystals embedded in amorphous silicon nitride matrix," *Appl. Phys. Lett.*, vol. 86, no. 19, pp. 193506-1–193506-3, May 2005.

[8] A. Benami, G. Santana, A. Ortiz, A. Ponce, D. Romeu, J. Aguilar-Hernández, G. Contreras-Puente, and J. C. Alonso, "Strong white and blue photoluminescence from silicon nanocrystals in SiN_x grown by remote PECVD using $SiCl_4/NH_3$," *Nanotechnology*, vol. 18, no. 15, p. 155 704, Apr. 2007.

[9] B. Gelloz, H. Sano, R. Boukherroub, D. D. M. Wayner, D. J. Lockwood, and N. Koshida, "Stabilization of porous silicon electroluminescence by surface passivation with controlled covalent bonds," *Appl. Phys. Lett.*, vol. 83, no. 12, pp. 2342–2344, Sep. 2003.

[10] G.-R. Lin, C. J. Lin, and C. K. Lin, "Enhanced Fowler–Nordheim tunneling effect in nanocrystallite Si based LED with interfacial Si nano-pyramids," *Opt. Exp.*, vol. 15, no. 5, pp. 2555–2563, Mar. 2007.

[11] S. S. Walavalkar, C. E. Hofmann, A. P. Homyk, M. D. Henry, H. A. Atwater, and A. Scherer, "Tunable visible and near-IR emission from sub-10 nm etched single-crystal Si nanopillars," *Nano Lett.*, vol. 10, no. 11, pp. 4423–4428, Nov. 2010.

[12] R. J. Walters, J. Kalkman, A. Polman, H. A. Atwater, and M. J. A. de Dood, "Photoluminescence quantum efficiency of dense silicon nanocrystal ensembles in SiO_2," *Phys. Rev. B*, vol. 73, no. 13, pp. 132302-1–132302-4, Apr. 2006.

[13] G. Ledoux, O. Guillois, D. Porterat, C. Reynaud, F. Huisken, B. Kohn, and V. Paillard, "Photoluminescence properties of silicon nanocrystals as function of their size," *Phys. Rev. B*, vol. 62, no. 23, pp. 15 942–15 951, Dec. 2000.

[14] L. Mangolini and U. Kortshagen, "Plasma-assisted synthesis of silicon nanocrystals inks," *Adv. Mater.*, vol. 19, no. 18, pp. 2513–2519, Sep. 2007.

[15] L. Pavesi and R. Turan, *Silicon Nanocrystals: Fundamentals, Synthesis, and Applications*. Weinheim, Germany: Wiley-VCH Verlag GmbH & Co. KGaA, 2010, pp. 465–469.

[16] G.-R. Lin, C. J. Lin, and H. C. Kuo, "Improving carrier transport and light emission in a silicon-nanocrystal based MOS light-emitting diode on silicon nanopillar array," *Appl. Phys. Lett.*, vol. 91, no. 9, pp. 093122-1–093122-3, Aug. 2007.

[17] N. M. Park, T. S. Kim, and S. J. Park, "Band gap engineering of amorphous silicon quantum dots for light-emitting diodes," *Appl. Phys. Lett.*, vol. 78, no. 17, pp. 2575–2577, Apr. 2001.

[18] K. S. Cho, N. M. Park, T. Y. Kim, K. H. Kim, G. Y. Sung, and J. H. Shin, "Erratum: 'High efficiency visible electroluminescence from silicon nanocrystals embedded in silicon nitride using a transparent doping layer' [Appl. Phys. Lett. 86, 071909 (2005)]," *Appl. Phys. Lett.*, vol. 88, no. 20, p. 209 904, May 2006.

[19] F. Iacona, D. Pacifici, A. Irrera, M. Miritello, G. Franzo, F. Priolo, D. Sanfilippo, G. D. Stefano, and P. G. Fallica, "Electroluminescence at 1.54 μm in Er-doped Si nanocluster-based devices," *Appl. Phys. Lett.*, vol. 81, no. 17, pp. 3242–3244, Oct. 2002.

[20] A. Marconi, A. Anopchenko, M. Wang, G. Pucker, P. Bellutti, and L. Pavesi, "High power efficiency in Si-nc/SiO_2 multilayer light emitting devices by bipolar direct tunneling," *Appl. Phys. Lett.*, vol. 94, no. 22, pp. 221110-1–221110-3, Jun. 2009.

[21] G.-R. Lin, C.-K. Lin, L.-J. Chou, and Y.-L. Chueh, "Synthesis of Si nanopyramids at SiO_x/Si interface for enhancing electroluminescence of Si-rich SiO_x," *Appl. Phys. Lett.*, vol. 89, no. 9, pp. 093126-1–093126-3, Aug. 2006.

[22] L. Rebohle, J. V. Borany, R. A. Yankov, W. Skorupa, I. E. Tyschenko, H. Frob, and K. Leo, "Strong blue and violet photoluminescence and electroluminescence from germanium-implanted and silicon-implanted silicon-dioxide layers," *Appl. Phys. Lett.*, vol. 71, no. 19, pp. 2809–2811, Nov. 1997.

[23] S. Fujita and N. Sugiyama, "Visible light-emitting devices with Schottky contacts on an ultrathin amorphous silicon layer containing silicon nanocrystals," *Appl. Phys. Lett.*, vol. 74, no. 2, pp. 308–310, Jan. 1999.

[24] N. Lalic and J. Linnros, "Light emitting diode structure based on Si nanocrystals formed by implantation into thermal oxide," *J. Lumin.*, vol. 80, no. 1–4, pp. 263–267, Dec. 1998.

[25] P. Photopoulos and A. G. Nassiopoulou, "Room- and low-temperature voltage tunable electroluminescence from a single layer of silicon quantum dots in between two thin SiO_2 layers," *Appl. Phys. Lett.*, vol. 77, no. 12, pp. 1816–1818, Sep. 2000.

[26] A. Irrera, D. Pacifici, M. Miritello, G. Franzo, F. Priolo, F. Iacona, D. Sanfilippo, G. D. Stefano, and P. G. Fallica, "Excitation and de-excitation properties of silicon quantum dots under electrical pumping," *Appl. Phys. Lett.*, vol. 81, no. 10, pp. 1866–1868, Sep. 2002.

[27] J. Valenta, R. Juhasz, and J. Linnros, "Photoluminescence spectroscopy of single silicon quantum dots," *Appl. Phys. Lett.*, vol. 80, no. 6, pp. 1070–1072, Feb. 2002.

[28] G. Franzo, A. Irrera, E. C. Moreira, M. Miritello, F. Iacona, D. Sanfilippo, G. Di Stefano, P. G. Fallica, and F. Priolo, "Electroluminescence of silicon nanocrystals in MOS structures," *Appl. Phys. A*, vol. 74, no. 1, pp. 1–5, 2002.

[29] C. Delerue, G. Allan, and M. Lannoo, "Theoretical aspects of the luminescence of porous silicon," *Phys. Rev. B*, vol. 48, no. 15, pp. 11 024–11 036, Oct. 1993.

[30] J. C. Cheang-Wong, A. Oliver, J. Roiz, J. M. Hernandez, L. Rodrigues-Fernandez, J. G. Morales, and A. Crespo-Sosa, "Optical properties of Ir^{2+}-implanted silica glass," *Nucl. Instrum. Methods Phys. Res. B, Beam Interact. Mater. At.*, vol. 175–177, pp. 490–494, Apr. 2001.

[31] H. S. Bae, T. G. Kim, C. N. Whang, S. Im, J. S. Yun, and J. H. Song, "Electroluminescence mechanism in SiO_x layers containing radiative centers," *J. Appl. Phys.*, vol. 91, no. 7, pp. 4078–4081, Apr. 2002.

[32] P. Mutti, g. Ghislotti, S. Bertoni, L. Bonoldi, G. F. Cerofolini, L. Meda, E. Grilli, and M. Guzzi, "Room-temperature visible luminescence from Si nanocrystals in Si implanted SiO_2 layers," *Appl. Phys. Lett.*, vol. 66, no. 7, pp. 851–853, Feb. 1995.

[33] T. Noma, K. S. Seol, H. Kato, M. Fujimaki, and Y. Ohki, "Origin of photoluminescence around 2.6–2.9 eV in silicon oxynitride," *Appl. Phys. Lett.*, vol. 79, no. 13, pp. 1995–1997, Sep. 2001.

[34] S. V. Deshpande, E. Gulari, S. W. Brown, and S. C. Rand, "Optical properties of silicon nitride films deposited by hot filament chemical vapor deposition," *J. Appl. Phys.*, vol. 77, no. 12, pp. 6534–6541, Jun. 1995.

[35] V. A. Belyakov, V. A. Burdov, R. Lockwood, and A. Merdrum, "Silicon nanocrystals: Fundamental theory and implications for stimulated emission," *Adv. Opt. Technol.*, vol. 2008, p. 279 502, Jan. 2008.

[36] D. Pi, R. W. Liptak, J. Deneen Nowak, N. P. Wells, C. B. Carter, S. A. Campbell, and U. Kortshagen, "Air-stable full-visible-spectrum emission from silicon nanocrystals synthesized by an all-gas-phase plasma approach," *Nanotechnology*, vol. 19, no. 24, p. 245 603, Jun. 2008.

[37] W. D. A. M. de Boer, D. Timmerman, K. Dohnalova, I. N. Yassievich, H. Zhang, W. J. Buma, and T. Gregorkiewicz, "Red spectral shift and enhanced quantum efficiency in phonon-free photoluminescence from silicon nanocrystals," *Nat. Nanotechnol.*, vol. 5, no. 12, pp. 878–884, Nov. 2010.

[38] H. Nishikawa, R. E. Stahlbush, and J. H. Stathis, "Oxygen-deficient centers and excess Si in buried oxide using photoluminescence spectroscopy," *Phys. Rev. B*, vol. 60, no. 23, pp. 15 910–15 918, Dec. 1999.

[39] G.-R. Lin, C.-J. Lin, and K.-C. Yu, "Time-resolved photoluminescence and capacitance–voltage analysis of the neutral vacancy defect in silicon implanted SiO_2 on silicon substrate," *J. Appl. Phys.*, vol. 96, no. 5, pp. 3025–3027, Sep. 2004.

[40] C.-J. Lin, C.-K. Lee, E. W. G. Diau, and G.-R. Lin, "Time-resolved photoluminescence analysis of multidose Si-Ion-implanted SiO_2," *J. Electrochem. Soc.*, vol. 153, no. 2, pp. E25–E32, 2006.

[41] Y. Liu, T. P. Chen, Y. Q. Fu, M. S. Tse, J. H. Hsieh, P. F. Ho, and Y. C. Liu, "A study on Si nanocrystal formation in Si-implanted SiO_2 films by X-ray photoelectron spectroscopy," *J. Phys. D, Appl. Phys.*, vol. 36, no. 19, pp. L97–L100, Oct. 2003.

[42] B. H. Augustine, E. A. Irene, Y. J. He, K. J. Price, L. E. McNeil, K. N. Christensen, and D. M. Maher, "Visible light emission from thin films containing Si, O, N, and H," *J. Appl. Phys.*, vol. 78, no. 6, pp. 4020–4030, Sep. 1995.

[43] W. Zhang, "Microstructural modification of nc-Si/SiO_x films during plasma-enhanced chemical vapor deposition," *Phys. Stat. Sol. (A)*, vol. 202, no. 9, pp. 1773–1777, Jul. 2005.

[44] S. Kim, M. C. Kim, S. H. Choi, K. J. Kim, H. N. Hwang, and C. C. Hwang, "Size dependence of Si2*p* core-level shift at Si nanocrystal/SiO_2 interfaces," *Appl. Phys. Lett.*, vol. 91, no. 10, pp. 103113-1–103113-3, Sep. 2007.

[45] B. H. Lai, C. H. Cheng, Y. H. Pai, and G. R. Lin, "Plasma power controlled deposition ofSiO_x with manipulated Si Quantum Dot size for photoluminescent wavelength tailoring," *Opt. Express*, vol. 18, no. 5, pp. 4449–4456, Mar. 2010.

[46] G. Chakraborty, S. Chattopadhyay, C. K. Sarkar, and C. Pramanik, "Tunneling current at the interface of silicon and silicon dioxide partly embedded with silicon nanocrystals in metal oxide semiconductor structures," *J. Appl. Phys.*, vol. 101, no. 2, pp. 024315-1–024315-6, Jan. 2007.

[47] T. Creazzo, B. Redding, E. Marchena, J. Murakowski, and D. W. Prather, "Tunable photoluminescence and electroluminescence of size-controlled silicon nanocrystals in nanocrystalline-Si/SiO_2 superlattices," *J. Lumin.*, vol. 130, no. 4, pp. 631–636, Apr. 2010.

[48] W. L. Hsu, Y. H. Pai, F. S. Meng, C. W. Liu, and G. R. Lin, "Nanograin crystalline transformation enhanced UV transparency of annealing refined indium tin oxide film," *Appl. Phys. Lett.*, vol. 94, no. 23, pp. 231906-1–231906-3, Jun. 2009.